Study of Linear Response in Rarita-Schwinger-Weyl Semimetals

Dissertation submitted to

Visvesvaraya National Institute of Technology, Nagpur

in partial fulfillment of the requirements for the award of the degree

Master of Science in Physics

by

Mahbub Alam

under the guidance of

Dr. Sayandip Ghosh

Department of Physics

Visvesvaraya National Institute of Technology, Nagpur

Nagpur 440 010, India

May 2025

Study of Linear Response in Rarita-Schwinger-Weyl Semimetals

Dissertation submitted to

Visvesvaraya National Institute of Technology, Nagpur

in partial fulfillment of the requirements for the award of the degree

Master of Science in Physics

by

Mahbub Alam

under the guidance of

Dr. Sayandip Ghosh

Department of Physics

Visvesvaraya National Institute of Technology, Nagpur

Nagpur 440 010, India

May 2025

©- Visvesvarya National Institute Of Technology(VNIT), 2025

Department of Physics

Visvesvaraya National Institute of Technology, Nagpur

Dissertation Approval Sheet

Dissertation entitled "Study of Linear Response in RSW Semimetal" by Mahbub Alam Enrollment No. **MS23PHY017** ID No. 30641 is approved for the degree of Master of Science in Physics

---

Name:
Supervisor

Name:
External Examiner

Name:
Chairman

Department of Physics
Visvesvaraya National Institute of Technology, Nagpur

Declaration

I, **Mahbub Alam**, hereby declare that this dissertation titled **"Study of Linear Response in RSW Semimetal"** is carried out by me in the Department of Physics of Visvesvaraya National Institute of Technology, Nagpur. The work is original and has not been submitted earlier whole or in part for the award of any degree/diploma at this or any other Institution / University.

Mahbub Alam
Date:

Certificate

This is to certify that the dissertation titled **"Study of Linear Response in RSW Semimetal"** is submitted by **Mahbub Alam** in partial fulfillment of the requirements for the award of the degree of **Master of Science in Physics**, VNIT Nagpur. The work is comprehensive, complete and fit for final evaluation.

Head, Department of Physics
VNIT, Nagpur
Date:

Supervisor,
Dr. Sayandip Ghosh
Assistant Professor
Dept. of Physics, VNIT, Nagpur

Visvesvaraya National Institute of Technology, Nagpur

Non- Plagiarism Certificate

I, **Mahbub Alam**, hereby declare that this dissertation titled **"Study Of Linear Response in RSW Semimetal"** is carried out by me in the Department of Physics of Visvesvaraya National Institute of Technology, Nagpur. The work is original and has not been submitted earlier whole or in part for the award of any degree/diploma at this or any other Institution / University.

Mahbub Alam
Date:

Dr. Sayandip Ghosh
Assistant Professor
Department of Physics,
VNIT, Nagpur

ORIGINALITY REPORT

10%	7%	9%	0%
SIMILARITY INDEX	INTERNET SOURCES	PUBLICATIONS	STUDENT PAPERS

ACKNOWLEDGEMENT

I would like to express my appreciation to **Dr. Sayandip Ghosh**, my project mentor and Assistant Professor in the Department of Physics at **Visvesvaraya National Institute of Technology (VNIT), Nagpur**, for inspiring me and helping me with my project work. If I did not give him a special thank you, I would be wasting my time. Having him as my guide makes me feel incredibly obligated. He has always been my support system and for that I am incredibly thankful. It has been a privilege to collaborate with him.

I would also like to express my gratitude to **Dr. B. R. Sankapal**, Head of the Department of Physics at **VNIT Nagpur**, and all of the lecturers for their invaluable collaboration and support during the session.

I would also like to express my heartfelt gratitude to my parents, **Mr. Alauddin Ansari** and **Mrs. Jahirun Nesha**, whose unwavering support, encouragement, and blessings have been the foundation of my academic journey. Their constant faith in me has been a source of strength and motivation throughout this project.

Mahbub Alam
MS23PHY017

en

ABSTRACT

Rarita-Schwinger-Weyl Semmetals have emerged as a new and interesting subject in solid state physics, where quasiparticles of spin-3/2 behaves according to the relativistic fermions. Using Kubo formula, we make low-energy-effective Hamiltonian which is responsible for the spin-3/2 fermions. After this, we have done the calculations for current-current correlation functions, for which the charge response function is calculated.From these calculations we find that the response characteristics of the RSW semimetals. This work proves that higher spin quasiparticles (spin-3/2) cause unique electromagnetic behavior in RSW semimetals. This theoretical study may be useful in the future for the design of quantum materials of spin-3/2.

List of Figures

1.1 Filling of the electronic states in various types of materials at equilibrium. Here, height is energy while width is the density of available states for a certain energy. 6

1.2 Schematic of topological semimetals with different dimensions and degeneracy, (a) 0D Weyl semimetal with two fold degenerate in which weyl nodes are connected by fermi arc.(b) Four fold dengenerate 0D Dirac semimetal.(c) Multifold degenerate weyl semi metal with 0D 3,6 and 8 fold-degenerate weyl nodes.(d) 1D Weyl nodal line semimetal with twofold.(e) 1D Dirac nodal line semimetal with four fold.(f) 2D Nodal surface semimetal with twofold. [3] . 7

1.3 The diamond lattice's insulating, Weyl, and Dirac phases. (1) A four-dimensional projective representation of the small group at X, which includes a fourfold rotation and a sublattice exchange operation, is covered by the states at the Dirac point at X. (2) A little inversion breaking perturbation causes four Weyl points on the zone face. Every Weyl point has its Chern number displayed. (3) For a T-breaking Zeeman field B orientated along the X-W line, two Weyl points show up on that line. By sufficiently disrupting rotational symmetry that no two-dimensional representations are permitted, B orientated in other orientations gaps all of the Dirac points. (4) Gapped phase produced by applying a magnetic field in any direction other than along x, y, or z, or by breaking the fourfold rotation symmetry. A normal, strong, or weak topological insulator can be the insulating phase [9]. 11

1.4 Graph of energy vs k in RSW semimetals. 12

1.5 Energy dispersion p for multi-Weyl fermions in the (p_x, p_y) plane for (a) $n = 1$, (b) $n = 2$, and (c) $n = 3$ around a Weyl node. For $n = 1$, 2, and 3, the valence and conduction bands display linear, quadratic, and cubic touching in this plane, respectively. However, the dispersion always scales linearly with p_z irrespective of n, as shown in (d). The momentum p is measured from the Weyl nodes, placed at $p = 0$. [1] 14

1.6 Brillouin zone (BZ) and crystal structure. (a) TaAs's crystal symmetry. (b) The bulk BZ and the projected surface BZ for both (001) and (100) surfaces. (c) The band structure of TaAs calculated by GGA without including the spin-orbit coupling. (d) The band structure of TaAs calculated by GGA with the spin-orbit coupling [6]. 16

Contents

1 Introduction **6**

1.1 Topological Semimetal 6

1.1.1 Weyl Semimetal 8

1.1.2 Dirac Semimetal 9

1.1.3 RSW Semimetal 10

1.1.4 Multi-Weyl Semimetal 13

1.1.5 Experimental Discovery of Weyl Semimetal TaAs 14

1.2 Motivation and Objective 16

2 Concepts and Methodology **17**

2.1 Linear Response 17

2.1.1 Basic Concept 17

2.1.2 Kubo Formula 18

2.1.3 Calculation of Physical quantities 19

2.1.4 Methodology of Charge Response 20

2.1.4.1 Start from the Unperturbed System 20

2.1.4.2 Introduce a Perturbation 21

2.1.4.3 Linear Response Approximation 21

2.1.4.4 Define the Charge Susceptibility (Response Function) . . . 21

2.1.4.5 Calculate Response function $\chi(\mathbf{q},\omega)$ 22

2.1.4.6 Compute Observable Quantities 22

3 Calculation of Linear response of Rarita-Schwinger Weyl Semimetals **23**

3.1 Linear response for RSW Semimetals 23

3.1.1 Calculation for charge response 25

4 Summary and conclusion **33**

Chapter 1

Introduction

1.1 Topological Semimetal

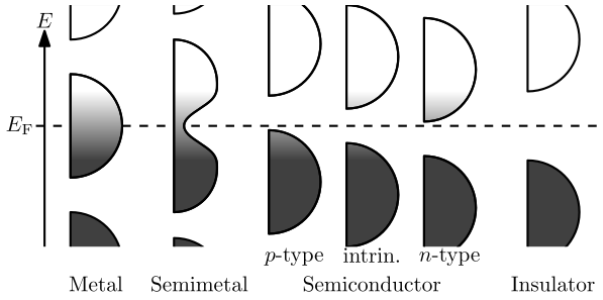

Figure 1.1: Filling of the electronic states in various types of materials at equilibrium. Here, height is energy while width is the density of available states for a certain energy.

An ordinary semimetal is a material whose conductivity lies between metals and semiconductor. Their electronic structure arises from a slight overlap of the conduction and valence bands in momentum space (Fig. 1.1); therefore, there is a small density of state near the Fermi level. An ordinary semimetal has some special property which is useful both in reserch and certain technological applications, e.g: because of the high mobility of the charge carrier this material can conduct electricity very effectively. Material like Bismuth (Bi) is an important example of this.

Despite its many useful properties, it also has many limitations. Their most important drawback is that there is no topological protection in their band structure, so their properties can be easily affected by external influences such as pressure, temperature and doping. Further, there is low carrier density, therefore their electrical conductivity may

be limited in certain applications. Therefore, currently the focus of research has shifted towards topological materials.

The study of electronic structure of topological materials has become a major area in modern condensed matter physics and has attracted enormous attention in the past decade. Recently, the research has expanded from topological insulator to topological semimetals. Topological semimetals has defined as a system where the conduction band and valance band touches at isolated points (nodes) at the fermi level in momentum space. In three-dimension (3D) momentum space, the valance and conduction bands cross each other either in zero-dimension (0D) at a point (node), in one-dimension along a line or curve or in two-dimension (2D) along the surface. In topological semimetal, the band crossing does not destroy easily by small perturbation because small perturbation can not brake any symmetries. [3]

Based on dimension and degeneracy, the topological semimetals can be divided into 0D nodal point semimetal (including Weyl semimetals, Diarac semimetals, Multidegenerate semimetal), 1D nodal line semimetal, and 2D surface semimetal, as shown in Fig:1.2.

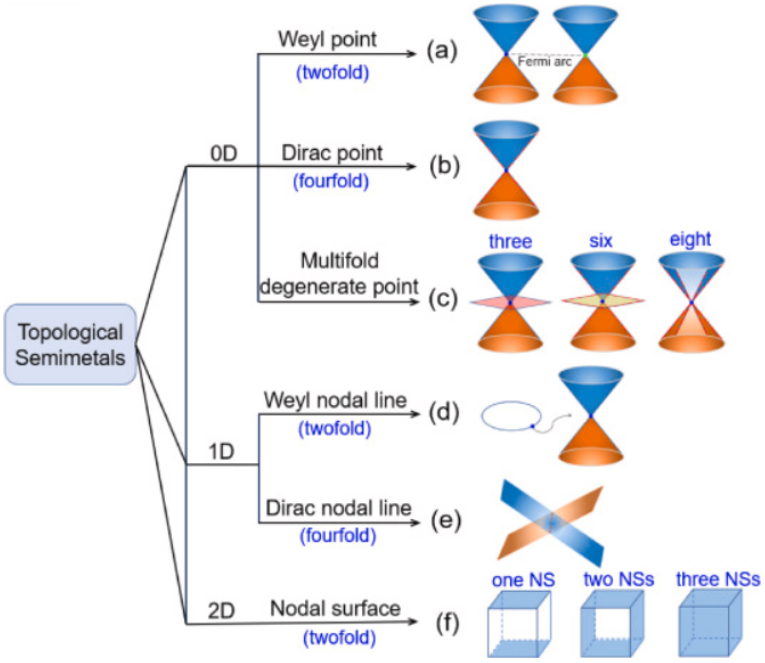

Figure 1.2: Schematic of topological semimetals with different dimensions and degeneracy, (a) 0D Weyl semimetal with two fold degenerate in which weyl nodes are connected by fermi arc.(b) Four fold dengenerate 0D Dirac semimetal.(c) Multifold degenerate weyl semi metal with 0D 3,6 and 8 fold-degenerate weyl nodes.(d) 1D Weyl nodal line semimetal with twofold.(e) 1D Dirac nodal line semimetal with four fold.(f) 2D Nodal surface semimetal with twofold. [3]

1.1.1 Weyl Semimetal

In a weyl semimetals two energy band cross each other at a point in momentum space, this intersection point is called weyl node, these weyl nodes can be described by weyl equation and due to unique topological surface states, these weyl nodes has become a subject of great interest. The weyl nodes always come in pair with opposite chirality left handed (LH) and right handed (RH), eg: if chirality is +1, the direction of spin is in the direction of momentum but if chirality is -1 then the direction of spin is in the opposite direction of momentum. The weyl nodes act as a magnetic monopole or source of Berry curvature in momentum space [7].

The characteristics of weyl semimetals is that every weyl nodes are connected by weyl fermi arc (Fig:1.1) which can seen by angle resolved photoemission spectroscopy (ARPES). The second important characteristics is that which arises due to topological charge on weyl point. In weyl semimetal, many novel transport phenomena related to chiral anamoly can be seen, eg: negative longitudinal magnetoresistance (NLMR), optical geometory and planar hall effect (PHE). Therefore, to trace the events, like that negative LMR has becomes a common method for identifying the presence of weyl nodes.

Here we explain in detail why chiral anamoly in weyl semiometal usually produces negative LMR. Chiral anamoly, which is also known as the Adler-Bell-Jackiw anomaly, means that the violations of the conservation for number of fermions of different chirality mean that the electric and magnetic fields are parallel to each other then pump the weyl fermions between weyl nodes of opposite chirality.

Although, ordinary metals and semiconductor, MR is usually positive,weak and not very sensitive towards the direction of magnetic field. LMR gives the significance of presence of weyl nodes in any metals

Space inversion symmetry, time-reversal symmetry, or both space-inversion and time-reversal symmetries must be broken in order for Weyl points to exist. Since Bloch electron interaction between bands causes Berry curvature, Weyl semimetal's inherent mechanism frequently results in a strong anomalous hall effect (AHE) during breaking time inversion. Additionally, magnetism can open up new options for Weyl semimetals because symmetry depends heavily on the direction of the magnetic moment and the spin-orbit coupling (SOC). More novel topological features may emerge, or the quantity

and location of weyl points may vary depending on the direction of magnetization.
The anomaly arises due to the interaction of block electrons between the bands, therefore, in weyl semimetals a strong anamalous hall effect (AHE) is seen due to the broken of TRS [5]. Additionally,magnetism opens up new possibilities for weyl semimetals because symmetries largely depend on the direction of magnetic moment and spin-orbit coupling (SOC). A change in the direction of the magnetic field may not only change the number and position of the weyl points but also give rise to some topological properties.
Weyl Semimetals plays a fundametal role in the development of topological semimetals (TSM). The range of magnetic order of weyl semimetals is greater than the nonmagnetic weyl semimetals. [3]

1.1.2 Dirac Semimetal

Topological Dirac semimetals (TDSMs) are most interesting topic for research in which the valance bands and conduction bands touch at discreate points in momentum space, these points of interaction are called Dirac points.Dirac points are four fold degenerate in momentum space.
Spinless graphene in 2D exhibits such point like degeneracy when conduction and valance band touch each other in momentum space.At Dirac points the low energy effective theory takes fallow a dirac equation -

$$\hat{H}(\mathbf{k}) = v(k_x\sigma_x + k_y\sigma_y) \tag{1.1}$$

where $\vec{\sigma} = \{\sigma_x, \sigma_y, \sigma_z\}$ are the Pauli matrices and $v \neq 0$. The presence of Dirac points near the fermi level is responsible for important characteristics of the graphene , for example:High electron mobility and conductivity. These Dirac points are not robust through as a disturbance proportional to σ_z can gap them.Spin-orbit coupling doubles the number of states; However the atoms of carbon are light so splitting is very small.
In 3D the generalised Hamiltonian is-

$$\hat{H}(\mathbf{k}) = v_{ij}k_i\sigma_j \tag{1.2}$$

when $|v_{ij}| \neq 0$,then $\hat{H}(\mathbf{k})$ become strong against perturbation because of three pauli matrices. This Hamiltonian is called Weyl Hamiltonian.

The strength of weyl points can be measured by Chern number of valance band (VB). The chern number of VB on a sphere surrounding the point can be measured strength of weyl point; which takes the value, $(\det[v_{ij}]) = \pm 1$. If a weyl node exist at some BZ momentum $\mathbf{k}$ the TRS demands that there exist another weyl point with some chern number of $-\mathbf{k}$. However, at the fermi level total Chern number should be zero. Therefore the presence of two more weyl points with opposite number at $\mathbf{k}'$ and $-\mathbf{k}'$ is necessary. In the presence of inversion symmetry the Chern number of weyl points at $\mathbf{k}$ and $-\mathbf{k}$ will be opposite to each other. Hence under both TRS and inversion symmetries, $\mathbf{k}$=$\mathbf{k}'$ and effective Hamiltonian describes 4 linearly expanding bands around $\mathbf{k}$, such Hamiltonian is called Dirac Hamiltonian. However, it is not stable against perturbation. Since there are 4×4 Dirac matrices which can used to open gap at Dirac point.

The pointlike (Dirac) degeneracies make up the whole fermi surface of a dirac semimetal. If inversion symmetry is maintained, 3D DSMs exists when a material is in a state of phase transition between an topological insulator and normal insulator. since Dirac points are degenerate which is split into two weyl points and then WSMs are formed, if inversion and TRS is broken at transition point in [fig:1(c)]. The topological properties of points give rise to intriguing characteristics including fermi-arc and pressure induced anamalous Hall effect. Recent research shows that WSMs has been obtained from DSMs by breaking the inversion or TRS. [9]

1.1.3 RSW Semimetal

RSW semimetal is a special type of topological semimetal in which four bands in energy band struture intersect simultaneously at the nodal point. The spin of quasi-particle at

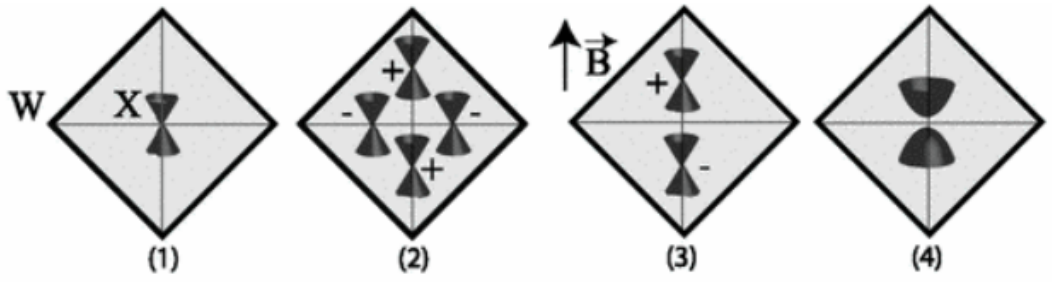

Figure 1.3: The diamond lattice's insulating, Weyl, and Dirac phases. (1) A four-dimensional projective representation of the small group at X, which includes a fourfold rotation and a sublattice exchange operation, is covered by the states at the Dirac point at X. (2) A little inversion breaking perturbation causes four Weyl points on the zone face. Every Weyl point has its Chern number displayed. (3) For a T-breaking Zeeman field B orientated along the X-W line, two Weyl points show up on that line. By sufficiently disrupting rotational symmetry that no two-dimensional representations are permitted, B orientated in other orientations gaps all of the Dirac points. (4) Gapped phase produced by applying a magnetic field in any direction other than along x, y, or z, or by breaking the fourfold rotation symmetry. A normal, strong, or weak topological insulator can be the insulating phase [9].

nodal point is $\frac{3}{2}$, which makes them special [4].

Some Important Points in RSW Semimetal

- In RSW semimetal weyl-fermions have spin 3/2, due to which their lower energy excitation becomes more complicated than traditional weyl semimetal.
- These semimetals indicate special type of topological properties, which are generated due to spin-3/2.
- Time-Reversal Symmetry,Crystal symmetries (such as cubic or tetrahedral symmetry) and inversion symmetry play an important role in these systems.
- The behaviour of particles near a fourfold band crossing can be described by the Hamiltonian :

$$H(\mathbf{k}) = v_o \left(k_x J_x + k_y J_y + \chi k_z J_z\right), \tag{1.3}$$

where v is the group velocity, $\vec{k}$ is the wave vector, and $\vec{J} = (J_x, J_y, J_z)$ are the 4×4 matrices corresponding to spin-$\frac{3}{2}$.

$$J_x = \frac{1}{2}\begin{pmatrix} 0 & \sqrt{3} & 0 & 0 \\ \sqrt{3} & 0 & 2 & 0 \\ 0 & 2 & 0 & \sqrt{3} \\ 0 & 0 & \sqrt{3} & 0 \end{pmatrix} \quad J_y = \frac{i}{2}\begin{pmatrix} 0 & -\sqrt{3} & 0 & 0 \\ \sqrt{3} & 0 & -2 & 0 \\ 0 & 2 & 0 & -\sqrt{3} \\ 0 & 0 & \sqrt{3} & 0 \end{pmatrix} \quad J_z = \begin{pmatrix} \frac{3}{2} & 0 & 0 & 0 \\ 0 & \frac{1}{2} & 0 & 0 \\ 0 & 0 & -\frac{1}{2} & 0 \\ 0 & 0 & 0 & -\frac{3}{2} \end{pmatrix}$$

The energy eigen values of $H(\mathbf{k})$ are as follows

$$E_s(k) = svk \quad \text{where} \quad s = \pm\tfrac{3}{2}, \pm\tfrac{1}{2}$$

, where $k = \sqrt{k_x^2 + k_y^2 + k_z^2}$. Which means

$$E_{3/2} = +\frac{3}{2}vk, E_{1/2} \quad = +\frac{1}{2}vk, E_{-1/2} = -\frac{1}{2}vk, E_{-3/2} \quad = -\frac{3}{2}vk.$$

This shows the four distinct energy branches.[2]

If we plot a graph between energy vs k then we get four straight lines which intersect at $k = 0$.

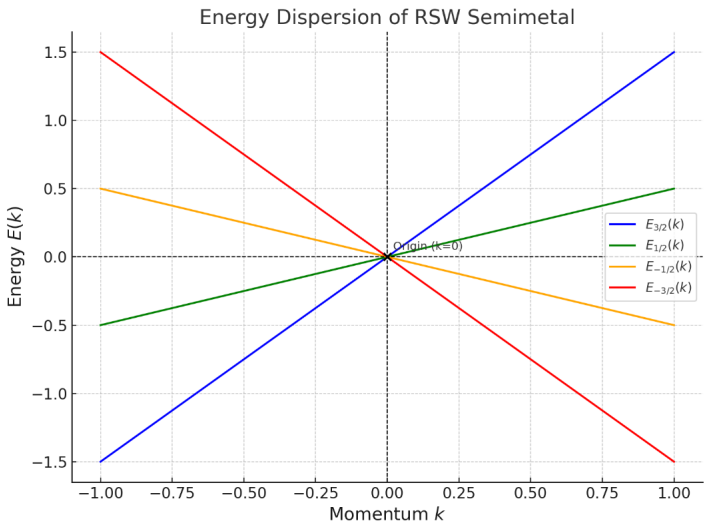

Figure 1.4: Graph of energy vs k in RSW semimetals.

1.1.4 Multi-Weyl Semimetal

To provide more depth to the concept of weyl semimetal, scientists conceived of such weyl nodes whose topological charge can be ± 2 or ± 3. These are called double or triple weyl nodes respectively, and the substances in which these nodes are found are called **Multi-Weyl Semimetals**. The composition of this type of semimetals is more complex than traditional weyl semimetals, and the dispersion of energy bands in them can cause quadratic or cubic rather than linear in one or two directions. Due to this discrepancy, special changes are seen in the electronic and topological characteristics of these substances. Thus, multi-weyl nodes introduce of a strong topological structure and can not be eliminated by small deflections untill their structural symmetry persists.

The presence of these weyl nodes produce specific states on the surface called Fermi Arcs. Traditional weyl semimetals contain a single Fermi arch on the surface of a weyl node that connects the nodes of different chirality. But in multi-weyl semimetles, due to high topological charge, These Fermi Arcs can be many or present in more complex form. This makes the surface physics richer and their investigation is possible by modern spectroscopy techniques.

The most important feature of multi-weyl semimetals is their an anisotropic dispersion. Traditional weyl semimetals have a linear relationship in all three directions, but in multi-weyl semimetals, there is a linear spread in one direction, while the other two directions are spread in quadratic or cubic. For example, if the dispersion is linear along the Z-axis and quadratic in the X-Y plane, the density of states and electronic velocity become dependent on the direction. Its effect can be seen on various physical properties such as electrical conductivity, magnetic reaction and sensitivity to light.

As far as real materials are concerned, Multi-Weyl semimetals have been predicted in many theoretical works. For example, $HgCr_2Se_4$ has been proposed as a double-Weyl semimetal. Similarly, the presence of triple-Weyl nodes in $SrSi_2$ has been predicted. However, their direct experimental confirmation is still limited. Consequently, Multi-Weyl band structures are artificially manufactured in structured systems such as photonic

crystals and artificial crystals of cold atomic gases. These platforms allow researchers to study the effects of Multi-Weyl nodes under ideal conditions.

The stability of these nodes depends on structural symmetries. A double-Weyl node is often shielded by fourfold rotational symmetry whereas triple-Weyl node might need sixfold symmetry. If these symmetry are broken-by stress or defect-then these multi-weyl nodes can divide into many single-weyl nodes. Therefore, their stability depends on the crystal structure.

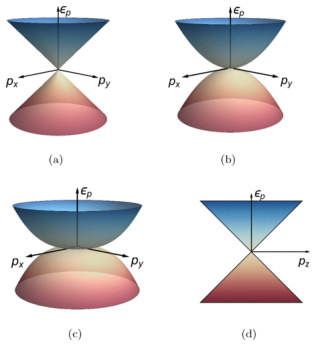

Figure 1.5: Energy dispersion p for multi-Weyl fermions in the (p_x, p_y) plane for (a) $n = 1$, (b) $n = 2$, and (c) $n = 3$ around a Weyl node. For $n = 1$, 2, and 3, the valence and conduction bands display linear, quadratic, and cubic touching in this plane, respectively. However, the dispersion always scales linearly with p_z irrespective of n, as shown in (d). The momentum p is measured from the Weyl nodes, placed at $p = 0$. [1]

1.1.5 Experimental Discovery of Weyl Semimetal TaAs

The journey to the discovery of TaAs began with theoretical predictions. In 2014-15, China's scientist Hungling Veng and his team calculated that the breaking of symmetry in the crystal structure (tetragonal system) of TaAs could be formed due to the breakdown of symmetry. This prediction was important because TaAs is a non-magnetic material, in which the time-reversal symmetry remains naturally, which is a necessary condition for the existence of weyl nodes. Subsequently, the team of Professor Zahid Hasan at Princeton University studied the electronic band structure of TaAs using angle-resolved photoemission spectroscopy (ARPES) technology. The results of the ARPES clearly showed the presence of weyl nodes and fermi arcs associated with them, which are the identity of weyl semimetals. This experiment in the magazine "Nature Physics" in 2015 published and it made TaAs the world's first experimentally confirmed the weyl

semimetals.

Many independent experiments were carried out in TaAs to confirm weyl Nodes. Scanning tunneling microscopy (STM) imagined the fermi arcs, which connects the two weyl nodes with opposite chirality. In addition, quantum oscillation experiments showed the effect of berry curvature in the electronic structure, which is the proof of the topological nature of weyl nodes. Transport measurement (such as magnetic resistance and hall effects) displayed the occurrence of "chiral anomaly", where resistance under parallel electrical and magnetic fields declines. The phenomenon is associated with the unique properties of weyl fermians and confirms the TaAs being a weyl semimetal [8].

The scientific impact of this discovery was profound. TaAs like weyl semimetals act as a bridge between topological insulators and conventional semimetals. Electrons show high mobility in these, which increase the possibility of growth of electronic devices with low energy consumption. Also, weyl nodes and Fermi Arcs can be used as topological cubits in quantum computing. After the discovery of TaAs, scientists identify other weyl semimetals (eg NbAs, $MoTe_2$), due to which this area is developing rapidly.

However, there are also challenges. It is difficult to manufacture and maintain their purity. Also, upgraded spectroscopy techniques are required to directly observe weyl nodes. In the future, researchers plan to study electronic interactions (such as superconductivity) and external effects (such as pressure or stress). The discovery of TaAs has not only deepened the understanding of topological substances, but it can also prove to be a cornerstone for future quantum technologies.
Thus, the experimental identity of tentlam arsenide has launched a new area in the field of weyl semimetal, which will deeply affect both science and technology. This discovery is a beautiful bridge between the fundamental principles of physics and their applications.

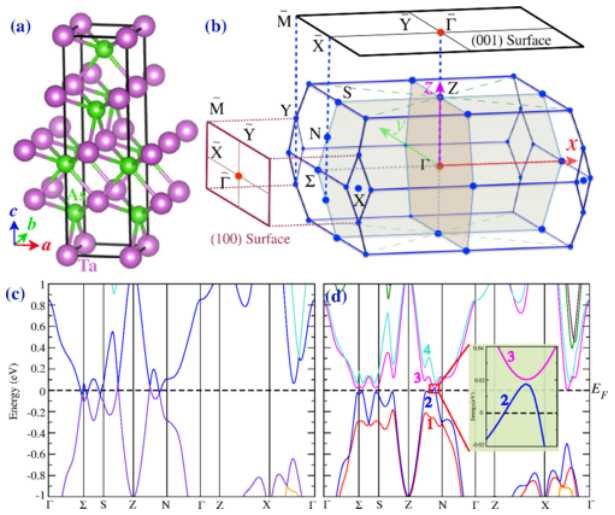

Figure 1.6: Brillouin zone (BZ) and crystal structure. (a) TaAs's crystal symmetry. (b) The bulk BZ and the projected surface BZ for both (001) and (100) surfaces. (c) The band structure of TaAs calculated by GGA without including the spin-orbit coupling. (d) The band structure of TaAs calculated by GGA with the spin-orbit coupling [6].

1.2 Motivation and Objective

The original attraction of the research of weyl and Multi-Weyl Semmetals is in those specific quantum properties hidden in these materials that make them completely different from normal metals or semimetals. They consist of special points called "weyl nodes", where energy bands join each other and form the basis of existence of particles such as weyl Fermions. These particles show unique chiral qualities (eg: right-left hand behavior) and extraordinary electronic conductivity. The goal of studying them is double: on the one hand, it is to highlight the new principles of quantum physics, on the other hand, their unprecedented electrical conductivity and stability in quantum computers, advanced sensors, or low -energy electronics have to use. Multiple nodes in multi-weyl semimetals increase their capacity, which makes them promising for future nanoscale technologies. Thus, this research not only deepens the theoretical understanding of science, but also the possibility of a revolution in the development of practical equipment.

Chapter 2

Concepts and Methodology

2.1 Linear Response

Physical systems, whether they are solids filled with electrons or gas of atoms, when subject to an external effect (such as electric field, magnetic field, thermal flow, etc.), they respond. If this external effect is very small, the system's reaction is linear - that is, the reaction is directly in proportion to the effect. In this situation, Linear Response Theory (LRT) is used. This theory is widely used in condensed matter physics, statistical mechanics, electromagnetic response, heat conductivity, and other transport phenomena. The principle is deeply connected to Fluctuation-Dissipation Theorem and is used in practical use through Green-Kubo Formula.

2.1.1 Basic Concept

Now we will discuss a general principle of this type of measurements. suppose, H_0 reflects the entire Hamiltonian that describes the system alone. One way to check the properties of the system is to connect it with an external weak perturbation (assuming that its

ground state is stable) and then see how the ground state and excited states are affected by that perturbation. Here $O(\mathbf{x}, t)$ represents a local observable, such as local density, charge current, or local magnetization. Now, when the system is gently added to an external deformity, the entire Hamiltonian H(t) can be written as

$$H(t) = H_0 + H_{\text{ext}}(t)$$

Here, $H_{\text{ext}}(t)$ is writtent as

$$H_{\text{ext}}(t) = \int d^3x\, O(\mathbf{x}, t) f(\mathbf{x}, t)$$

2.1.2 Kubo Formula

It explains that how much change will happen in a system (A) when a small perturbation apply on that system (A). Mathematically, it can be written as

$$\delta\langle A(\vec{x}, t)\rangle = \int d^3\vec{x}' \int_{-\infty}^{t} dt'\, \chi_{AO}(\mathbf{x}, t; \mathbf{x}', t') f(\mathbf{x}', t')$$
$$\text{or}, \delta\langle A(\mathbf{x}, t)\rangle = \int d^4x'\, \chi_{AO}(x, x') f(x')$$

where

$$d^4x' = d^3\mathbf{x}'\, dt'$$
$$\chi_{AO}(\mathbf{x}, \mathbf{x}') = \text{Response function}$$
$$f(\vec{x}') = \text{External perturbation at } (\vec{x}', t')$$

The integration over space and time is very complex so we use Fourier Transform of above integration which can be written as

$$\delta\langle A(\omega, \mathbf{q})\rangle = \chi_{AO}(\omega, \mathbf{q}) f(\omega, \mathbf{q})$$

where ω and q are angular frequency and momentum vector respectively

Response function ($\chi_{AO}(\vec{x}, \vec{x}')$)

Response function explains that what will be the effect of external perturbation (as ; electric field,magnetic fiels) on a system, it may be depend on position and time. Mathematically it can be written as

$$\chi_{AO}(\mathbf{x}, t; \mathbf{x}', t') = -\frac{\hbar}{i}\,\theta(t - t')\langle[A(\mathbf{x}, t), O(\mathbf{x}', t')]\rangle$$

Here $\theta(t - t')$ is a Heaviside step function which ensures that effect of perturbstion will be happen iff $t > t'$.

2.1.3 Calculation of Physical quantities

Here, we are using LRT and finding out that how a physical quantity (current) change due to external perturbation (As ; Electric Field)

Example: Response For Current Density

If you apply a small external electric field in a substance like RSW semimetal, then a current (J_i) is produce in it. This current is linear to applied field and it is expressed through conductivity tensor-

$$J_i(\omega) = \sigma_{ij}(\omega)E_j(\omega)$$

where

$$J_i(\omega) = \text{Current density at frequency } \omega \text{ in the } i\text{-th direction},$$
$$\sigma_{ij}(\omega) = \text{Element of the conductivity tensor},$$
$$E_j(\omega) = \text{External electric field at frequency } \omega \text{ in the } j\text{-th direction}.$$

Conductivity Tensor (σ_{ij})

It can be written by using **Kubo Formula** as

$$\sigma_{ij}(\omega) = \frac{1}{i\omega}\left[\Pi_{ij}(\omega) - \Pi_{ij}(0)\right]$$

where, $\Pi_{ij}(\omega)$ and $\Pi_{ij}(0)$ are the current-current correlation functions at frequencies ω and 0, respectively.

2.1.4 Methodology of Charge Response

The methodology of charging response is an theoretical and computational structure that is used to study the response of charged particles (such as electrons in solids), when an external electric field or potential is imposed on them. This study is often done in the structure of Linear Response theory and this is a fundamental concept in condensed matter physics and materials science.

2.1.4.1 Start from the Unperturbed System

We consider a quantum system in equilibrium, described by a Hamiltonian H_0 and a ground state wave function $|\Psi_0\rangle$.

The charge density $\rho(\mathbf{r})$ is given in this state.

2.1.4.2 Introduce a Perturbation

Now,we apply a weak, time-dependent external potential $V_{\text{ext}}(\mathbf{r}, t)$ that couples to the charge density:

$$H' = \int d^3r\, \rho(\mathbf{r}) V_{\text{ext}}(\mathbf{r}, t)$$

The total Hamiltonian becomes:

$$H(t) = H_0 + H'$$

2.1.4.3 Linear Response Approximation

If perturbation is small then the change in charge density $\delta\rho(\vec{r}, t)$ is linear with V_{ext}.

2.1.4.4 Define the Charge Susceptibility (Response Function)

If the density-density response function is $\chi(\mathbf{r}, \mathbf{r}'; t - t')$, then :

$$\delta\rho(\mathbf{r}, t) = \int d^3r' \int dt'\, \chi(\mathbf{r}, \mathbf{r}'; t - t') V_{\text{ext}}(\mathbf{r}', t')$$

In Fourier space (momentum and frequency):

$$\delta\rho(\mathbf{q}, \omega) = \chi(\mathbf{q}, \omega) V_{\text{ext}}(\mathbf{q}, \omega)$$

2.1.4.5 Calculate Response function $\chi(\mathbf{q}, \omega)$

(a) Non-interacting systems (Lindhard function):

$$\chi_0(\mathbf{q}, \omega) = \sum_{\mathbf{k}} \frac{f(\epsilon_{\mathbf{k}+\mathbf{q}}) - f(\epsilon_{\mathbf{k}})}{\hbar\omega + \epsilon_{\mathbf{k}} - \epsilon_{\mathbf{k}+\mathbf{q}} + i\eta}$$

(b) Interacting systems (Random Phase Approximation - RPA):

$$\chi(\mathbf{q}, \omega) = \frac{\chi_0(\mathbf{q}, \omega)}{1 - V(\mathbf{q})\chi_0(\mathbf{q}, \omega)}$$

Where $V(\mathbf{q})$ is the Fourier transform of the Coulomb interaction.

2.1.4.6 Compute Observable Quantities

From the charge response function, you can compute the following quantities

- **Dielectric function:**
$$\varepsilon(\vec{q}, \omega) = 1 - V(\vec{q})\chi_0(\vec{q}, \omega)$$
- **Plasmon dispersion:** Determined from the roots of
$$\varepsilon(\vec{q}, \omega) = 0$$
- **Screening behavior:** Describes how external charges are screened by the electron gas.

Chapter 3

Calculation of Linear response of Rarita-Schwinger Weyl Semimetals

3.1 Linear response for RSW Semimetals

In this chapter, we present the theoretical calculation of the charge response in RSW semimetals where low-energy quasiparticles have spin-3/2 . We use semiclassical boltzmann transport theory, which includes Berry Curvature and Orbital Magnetic Moment. These two topological properties (Topological features) specifically affect the electric current in the RSW semimetals.

In RSW semimetals, the behaviour of particles near a fourfold band crossing can be described by the Hamiltonian:

$$H(\mathbf{k}) = v_0 \left(k_x J_x + k_y J_y + \chi k_z J_z\right) \tag{3.1}$$

where $\mathbf{v_0}$ is the group velocity, $\mathbf{k}$ is the wave vector, and $\vec{J} = (J_x, J_y, J_z)$ are the 4×4

matrices corresponding to spin-$\frac{3}{2}$. The energy eigen values of H(k) are as follows

$$E_s(\mathbf{k}) = s\, v\, |\mathbf{k}| \quad \text{where} \quad s = \pm\tfrac{3}{2},\ \pm\tfrac{1}{2}.$$

which means:

$$E_{3/2} = +\tfrac{3}{2}\, v_0\, |\mathbf{k}|, \quad E_{1/2} = +\tfrac{1}{2}\, v_0\, |\mathbf{k}|,$$
$$E_{-1/2} = -\tfrac{1}{2}\, v_0\, |\mathbf{k}|, \quad E_{-3/2} = -\tfrac{3}{2}\, v_0\, |\mathbf{k}|.$$

This shows the four distinct energy branches[2].

The eigen vectors corresponding to each eigen values are

$$|\phi_{-\frac{3}{2}}\rangle = \begin{bmatrix} -e^{-3i\phi}\sin^3\left(\frac{\theta}{2}\right) \\ \sqrt{3}e^{-2i\phi}\sin^2\left(\frac{\theta}{2}\right)\cos\left(\frac{\theta}{2}\right) \\ -\sqrt{3}e^{-i\phi}\sin\left(\frac{\theta}{2}\right)\cos^2\left(\frac{\theta}{2}\right) \\ \cos^3\left(\frac{\theta}{2}\right) \end{bmatrix}, \qquad |\phi_{-\frac{1}{2}}\rangle = \begin{bmatrix} e^{-3i\phi}\cos^3\left(\frac{\theta}{2}\right) \\ \sqrt{3}e^{-2i\phi}\sin\left(\frac{\theta}{2}\right)\cos^2\left(\frac{\theta}{2}\right) \\ \sqrt{3}e^{-i\phi}\sin^2\left(\frac{\theta}{2}\right)\cos\left(\frac{\theta}{2}\right) \\ \sin^3\left(\frac{\theta}{2}\right) \end{bmatrix},$$

$$|\phi_{+\frac{1}{2}}\rangle = \begin{bmatrix} \sqrt{3}e^{-3i\phi}\sin^2\left(\frac{\theta}{2}\right)\cos\left(\frac{\theta}{2}\right) \\ -\frac{1}{2}e^{-2i\phi}(1+3\cos\theta)\sin\left(\frac{\theta}{2}\right) \\ \frac{1}{2}e^{-i\phi}\cos\left(\frac{\theta}{2}\right)(-1+3\cos\theta) \\ \sqrt{3}\sin\left(\frac{\theta}{2}\right)\cos^2\left(\frac{\theta}{2}\right) \end{bmatrix}, \quad |\phi_{+\frac{3}{2}}\rangle = \begin{bmatrix} -\sqrt{3}e^{-3i\phi}\sin\left(\frac{\theta}{2}\right)\cos^2\left(\frac{\theta}{2}\right) \\ \frac{1}{2}e^{-2i\phi}\cos\left(\frac{\theta}{2}\right)\cos\theta \\ \frac{1}{2}e^{-i\phi}(1+3\cos\theta)\sin\left(\frac{\theta}{2}\right) \\ \sqrt{3}\sin^2\left(\frac{\theta}{2}\right)\cos\left(\frac{\theta}{2}\right) \end{bmatrix}.$$

where, θ is the polar angle and ϕ is the azimuthal angle of $\mathbf{k}$.

3.1.1 Calculation for charge response

The charge response function is given by

$$\Pi_{00}(\mathbf{q}, i\omega_n) = -\frac{1}{N}\sum_{\mathbf{k}}\sum_{\lambda,\lambda'} \frac{\langle\phi_{\lambda'}(\mathbf{k}+\mathbf{q})|J_0|\phi_\lambda(\mathbf{k})\rangle\ \langle\phi_\lambda(\mathbf{k})|J_0|\phi_{\lambda'}(\mathbf{k}+\mathbf{q})\rangle}{i\omega_n + \epsilon_\lambda(\mathbf{k}) - \epsilon_{\lambda'}(\mathbf{k}+\mathbf{q})} \times \Big(n_F^{\lambda}(\mathbf{k}) - n_F^{\lambda'}(\mathbf{k}+\mathbf{q})\Big)\,, \tag{3.2}$$

where λ,$\lambda' = \pm\frac{1}{2},\pm\frac{3}{2}$ are band indices, $n_F^{\lambda}(\mathbf{k})$ and $n_F^{\lambda'}(\mathbf{k}+\mathbf{q})$ denote the usual Fermi–Dirac distribution functions for the bands λ and λ', respectively [1].

Using analytical continuation $i\omega_n \longrightarrow \omega + i\eta$ in the low-temperature limit, (3.2) becomes

$$\Pi_{00}(\mathbf{q}, \omega) = -\frac{1}{N}\sum_{\mathbf{k}}\sum_{\lambda,\lambda'} \frac{\langle\phi_{\lambda'}(\mathbf{k}+\mathbf{q})|J_0|\phi_\lambda(\mathbf{k})\rangle\ \langle\phi_\lambda(\mathbf{k})|J_0|\phi_{\lambda'}(\mathbf{k}+\mathbf{q})\rangle}{\omega + i\eta + \epsilon_\lambda(\mathbf{k}) - \epsilon_{\lambda'}(\mathbf{k}+\mathbf{q})} \times \big[n_F^{\lambda}(\mathbf{k}) - n_F^{\lambda'}(\mathbf{k}+\mathbf{q})\big] \tag{3.3}$$

We define the following equations

$$\cos(\theta_k)\cos(\theta_{k+q}) + \cos(\phi_k - \phi_{k+q})\sin(\theta_k)\sin(\theta_{k+q}) = \cos(\Theta) \tag{3.4}$$

$$\cos(\frac{\Theta}{2}) = C, \quad \sin(\frac{\Theta}{2}) = S \tag{3.5}$$

where Θ is the angle between the vectors $\mathbf{k}$ and $\mathbf{k}+\mathbf{q}$.

Then, we calculate various relevant terms in the denominator

(a) $\left\langle \phi_{\frac{k+q}{2}} \middle| J_0 \middle| \phi_{\frac{k}{2}} \right\rangle \cdot \left\langle \phi_{\frac{k}{2}} \middle| J_0 \middle| \phi_{\frac{k+q}{2}} \right\rangle$

$$= \frac{1}{8} \left(1 - 3\cos\theta\right)^2 \left(1 + \cos\theta\right)$$

$$= (1 - 3S^2)^2 C^2,$$

(b) $\left\langle \phi_{\frac{k+q}{2}} \middle| J_0 \middle| \phi_{-\frac{3k}{2}} \right\rangle \cdot \left\langle \phi_{-\frac{3k}{2}} \middle| J_0 \middle| \phi_{\frac{k+q}{2}} \right\rangle$

$$= \frac{3}{8} \left(\sin^2\theta\right) \left(1 + \cos\theta\right)$$

$$= 3S^2 C^4,$$

(c) $\left\langle \phi_{\frac{3(k+q)}{2}} \middle| J_0 \middle| \phi_{-\frac{3k}{2}} \right\rangle \cdot \left\langle \phi_{-\frac{3k}{2}} \middle| J_0 \middle| \phi_{\frac{3(k+q)}{2}} \right\rangle$

$$= \frac{1}{8} \left(\sin^2\theta\right) \left(1 + \cos\theta\right)$$

$$= 3S^4 C^2,$$

(d) $\left\langle \phi_{-\frac{3(k+q)}{2}} \middle| J_0 \middle| \phi_{-\frac{k}{2}} \right\rangle \cdot \left\langle \phi_{-\frac{k}{2}} \middle| J_0 \middle| \phi_{-\frac{3(k+q)}{2}} \right\rangle$

$$= -\frac{1}{8} \left(-1 + \cos\theta\right)^3$$

$$= S^6,$$

(e) $\left\langle \phi_{-\frac{3(k+q)}{2}} \middle| J_0 \middle| \phi_{\frac{k}{2}} \right\rangle \cdot \left\langle \phi_{\frac{k}{2}} \middle| J_0 \middle| \phi_{-\frac{3(k+q)}{2}} \right\rangle$

$$= \frac{3}{8} \left(\sin^2\theta\right) \left(1 + \cos\theta\right)$$

$$= 3S^2 C^4,$$

(f) $\left\langle \phi_{-\frac{3(k+q)}{2}} \middle| J_0 \middle| \phi_{-\frac{3k}{2}} \right\rangle \cdot \left\langle \phi_{-\frac{3k}{2}} \middle| J_0 \middle| \phi_{-\frac{3(k+q)}{2}} \right\rangle$

$$= \left(\cos^6 \frac{\theta}{2}\right)$$

$$= C^6,$$

(g) $\left\langle \phi_{\frac{3(k+q)}{2}} \middle| J_0 \middle| \phi_{\frac{k}{2}} \right\rangle \cdot \left\langle \phi_{\frac{k}{2}} \middle| J_0 \middle| \phi_{\frac{3(k+q)}{2}} \right\rangle$

$$= -\frac{1}{8}\left(-1+\cos\theta\right)\left(1+3\cos\theta\right)^2$$

$$= (1-3C^2)^2 S^2,$$

(h) $\left\langle \phi_{-\frac{(k+q)}{2}} \middle| J_0 \middle| \phi_{\frac{k}{2}} \right\rangle \cdot \left\langle \phi_{\frac{k}{2}} \middle| J_0 \middle| \phi_{-\frac{(k+q)}{2}} \right\rangle$

$$= \frac{1}{8}\left(\sin^2\theta\right)\left(1+\cos\theta\right)$$

$$= 3S^4C^2,$$

(i) $\left\langle \phi_{-\frac{3(k+q)}{2}} \middle| J_0 \middle| \phi_{\frac{3k}{2}} \right\rangle \cdot \left\langle \phi_{\frac{3k}{2}} \middle| J_0 \middle| \phi_{-\frac{3(k+q)}{2}} \right\rangle$

$$= \frac{1}{8}\left(\sin^2\theta\right)\left(1+\cos\theta\right)$$

$$= 3S^4C^2,$$

(j) $\left\langle \phi_{\frac{(k+q)}{2}} \middle| J_0 \middle| \phi_{\frac{3k}{2}} \right\rangle \cdot \left\langle \phi_{\frac{3k}{2}} \middle| J_0 \middle| \phi_{\frac{(k+q)}{2}} \right\rangle$

$$= -\frac{1}{8}\left(-1+\cos\theta\right)\left(1+3\cos\theta\right)^2$$

$$= (1-3C^2)^2 S^2,$$

(k) $\left\langle \phi_{\frac{3(k+q)}{2}} \middle| J_0 \middle| \phi_{\frac{3k}{2}} \right\rangle \cdot \left\langle \phi_{\frac{3k}{2}} \middle| J_0 \middle| \phi_{\frac{3(k+q)}{2}} \right\rangle$

$$= \frac{1}{8}\left(1-3\cos\theta\right)^2\left(1+\cos\theta\right)$$

$$= (1-3S^2)^2 C^2,$$

(l) $\left\langle \phi_{-\frac{k+q}{2}} \middle| J_0 \middle| \phi_{\frac{3k}{2}} \right\rangle \cdot \left\langle \phi_{\frac{3k}{2}} \middle| J_0 \middle| \phi_{-\frac{k+q}{2}} \right\rangle$

$$= \frac{3}{8}\left(\sin^2\theta\right)\left(1+\cos\theta\right)$$

$$= 3S^2C^4,$$

(m) $\left\langle \phi_{-\frac{(k+q)}{2}} \middle| J_0 \middle| \phi_{-\frac{3k}{2}} \right\rangle \cdot \left\langle \phi_{-\frac{3k}{2}} \middle| J_0 \middle| \phi_{-\frac{(k+q)}{2}} \right\rangle$

$$= -\frac{1}{8}\left(-1+\cos\theta\right)^3$$

$$= S^6,$$

(n) $\left\langle \phi_{\frac{(k+q)}{2}} \middle| J_0 \middle| \phi_{-\frac{k}{2}} \right\rangle \cdot \left\langle \phi_{-\frac{k}{2}} \middle| J_0 \middle| \phi_{\frac{(k+q)}{2}} \right\rangle$

$$= \frac{1}{8}\left(\sin^2\theta\right)\left(1+\cos\theta\right)$$

$$= 3S^4C^2,$$

(o) $\left\langle \phi_{\frac{3(k+q)}{2}} \middle| J_0 \middle| \phi_{-\frac{k}{2}} \right\rangle \cdot \left\langle \phi_{-\frac{k}{2}} \middle| J_0 \middle| \phi_{\frac{3(k+q)}{2}} \right\rangle$

$$= \frac{3}{8}\left(\sin^2\theta\right)\left(1+\cos\theta\right)$$

$$= 3S^2C^4,$$

(p) $\left\langle \phi_{-\frac{(k+q)}{2}} \middle| J_0 \middle| \phi_{-\frac{k}{2}} \right\rangle \cdot \left\langle \phi_{-\frac{k}{2}} \middle| J_0 \middle| \phi_{-\frac{(k+q)}{2}} \right\rangle$

$$= \left(\cos^6\frac{\theta}{2}\right)$$

$$= C^6,$$

Using Subsection (3.1.1) we define the matrix in $(\frac{3}{2}\ \frac{1}{2}\ -\frac{1}{2}\ -\frac{3}{2})$

$$\langle J_0(\theta_{\mathbf{k},\mathbf{k+q}})\rangle^2 = \begin{bmatrix} (1-3S^2)^2C^2 & (1-3C^2)^2S^2 & 3S^2C^4 & 3C^2S^4 \\ (1-3C^2)^2S^2 & (1-3S^2)^2C^2 & 3C^2S^4 & 3S^2C^4 \\ 3S^2C^4 & 3C^2S^4 & C^6 & S^6 \\ 3C^2S^4 & 3S^2C^4 & S^6 & C^6 \end{bmatrix}$$

Now, we calculate the charge response for interband processes

(a) For $\lambda' = -\frac{3}{2}, \quad \lambda = \frac{3}{2}$.

$$\begin{aligned}
\Pi_{\frac{3}{2},-\frac{3}{2}} &= \frac{1}{N}\sum \frac{3C^2S^4}{\frac{3}{2}|k+q| \pm (\omega + i\eta)} \\
&= \frac{1}{4\pi}\sum \frac{\sin\theta(1-\cos\theta)}{|k+q| \pm \left(\frac{\omega+i\eta}{v}\right)} \\
&= \frac{1}{4\pi v}\sum \frac{\sin\theta(1-\cos\theta)}{|k+q| \pm (\tilde{\omega} + i\eta)} \\
&= -\frac{\pi}{16Nq^2v}\int \frac{1}{k^2}\,dk \int \frac{(k'^2-(k-q)^2)(k+q)^2-k'^2)^2k'}{|k+q| \pm (\tilde{\omega}+i\eta)}dk'
\end{aligned}$$

Its imaginary part can be calculated easily and reads

$$\begin{aligned}
\mathrm{Im}\Pi_{\frac{3}{2},-\frac{3}{2}} = -\frac{\pi}{16Nq^2v}\Bigg[\frac{1}{6q}\Bigg\{ &(q-\tilde{\omega})\left(52\tilde{\omega} - 29q\tilde{\omega}^2 + 6\tilde{\omega}^3 + q^3(-17+\log 64)\right) \\
&+ 6q^3(q-\tilde{\omega})\log\left(\frac{q}{q-\tilde{\omega}}\right) - 6q\tilde{\omega}(2q+7\tilde{\omega})\log\left(\frac{2q}{q+\tilde{\omega}}\right)\Bigg\}\Bigg]
\end{aligned}$$

(b) For $\lambda' = -\frac{1}{2}, \quad \lambda = \frac{1}{2}$.

$$\begin{aligned}
\Pi_{\frac{1}{2},-\frac{1}{2}} &= \frac{1}{N}\sum \frac{3C^2S^4}{\frac{1}{2}|k+q| \pm (\omega + i\eta)} \\
&= \frac{3}{4\pi}\sum \frac{\sin\Theta(1-\cos\Theta)}{|k+q| \pm \left(\frac{\omega+i\eta}{v}\right)} \\
&= \frac{3}{4\pi v}\sum \frac{\sin\Theta(1-\cos\Theta)}{|k+q| \pm (\tilde{\omega} + i\eta)} \\
&= -\frac{3\pi}{16Nq^2v}\int \frac{1}{k^2}\,dk \int \frac{(k'^2-(k-q)^2)(k+q)^2-k'^2)^2k'}{|k+q| \pm (\tilde{\omega}+i\eta)}dk'
\end{aligned}$$

$$\mathrm{Im}\Pi_{\frac{1}{2},-\frac{1}{2}} = -\frac{3\pi}{16Nq^2v}\left[\frac{1}{6q}\Big\{(q-\tilde{\omega})\left(52\tilde{\omega}-29q\tilde{\omega}^2+6\tilde{\omega}^3+q^3(-17+\log 64)\right)\right.$$
$$\left.+\,6q^3(q-\tilde{\omega})\log\left(\frac{q}{q-\tilde{\omega}}\right)-6q\tilde{\omega}(2q+7\tilde{\omega})\log\left(\frac{2q}{q+\tilde{\omega}}\right)\Big\}\right]$$

(c) For $\lambda' = -\frac{1}{2}, \quad \lambda = \frac{3}{2}$.

$$\begin{aligned}\Pi_{\frac{3}{2},-\frac{1}{2}} &= \frac{3}{8N}\cdot\frac{2}{v}\sum\frac{\sin^2\Theta(1+\cos\Theta)}{|3k+k'|\mp\left(\frac{\omega+i\eta}{v}\right)}\\ &= \frac{3}{4Nv}\sum\frac{\sin^2\Theta(1+\cos\Theta)}{|3k+k'|\pm(\tilde{\omega}+i\eta)}\cdot v\\ &= -\frac{3\pi}{16Nvq^2}\int\frac{dk}{k^3}\cdot\int\frac{\left[(k-q)^2-k'^2\right]^2\cdot\left[(k+q)^2-k'^2\right]k'}{|3k+k'|\mp(\tilde{\omega}+i\eta)|}dk'\end{aligned}$$

For $k > q$:

$$\begin{aligned}\mathrm{Im}\Pi_{\frac{3}{2},-\frac{1}{2}} &= \frac{19q^6}{10}-\frac{487q^5\omega_p}{15}-\frac{13q^4\omega_p^2}{2}+76q^3\omega_p^3+4q^2\omega_p^4-42q\omega_p^5\\ &\quad+(3q-7\omega_p)(q-\omega_p)^2(q+\omega_p)^2(q+3\omega_p)\left[\log(-q+\omega_p)-\log(q+\omega_p)\right]\\ &\quad-\frac{(3q-\omega_p)}{480q}\Big(27171q^6-86385q^5\omega_p+105990q^4\omega_p^2-77290q^3\omega_p^3\\ &\qquad+43335q^2\omega_p^4-13077q\omega_p^5-480\omega_p^6\Big)\\ &\quad+(3q-7\omega_p)(q-\omega_p)^2(q+\omega_p)^2(q+3\omega_p)\cdot\log\left(\frac{4q}{q+\omega_p}\right)\end{aligned}$$

For $k < q$:

$$\begin{aligned}\mathrm{Im}\Pi_{\frac{3}{2},-\frac{1}{2}} = \frac{1}{480}(q-\omega_p)^2\Big(&1209q^4+2620q^3\omega_p-4654q^2\omega_p^2-13308q\omega_p^3-6987\omega_p^4\Big)\\ &-(3q-7\omega_p)(q+\omega_p)^2(q+3\omega_p)\cdot\log(2)\\ &+\frac{(5q-\omega_p)}{480q}\Big(16485q^6-57085q^5\omega_p+68830q^4\omega_p^2-46510q^3\omega_p^3\\ &\quad+32541q^2\omega_p^4-14037q\omega_p^5-480\omega_p^6\Big)\\ &-(3q-7\omega_p)(q-\omega_p)^2(q+\omega_p)^2(q+3\omega_p)\cdot\log\left(\frac{4q}{-q+\omega_p}\right)\end{aligned}$$

(d) For $\lambda'=-\frac{3}{2},\quad \lambda=\frac{1}{2}$.

$$\begin{aligned}\Pi_{\frac{3}{2},-\frac{1}{2}} &= \frac{3}{8N}\cdot\frac{2}{v}\sum\frac{\sin^2\Theta(1+\cos\Theta)}{|k+3k'|\mp\left(\frac{\omega+i\eta}{v}\right)}\\ &= \frac{3}{4Nv}\sum\frac{\sin^2\Theta(1+\cos\Theta)}{|3k+k'|\pm(\tilde{\omega}+i\eta)}\cdot v\\ &= -\frac{3\pi}{16Nvq^2}\int\frac{dk}{k^3}\cdot\int\frac{\left[(k-q)^2-k'^2\right]^2\cdot\left[(k+q)^2-k'^2\right]k'}{|3k+k'|\mp(\tilde{\omega}+i\eta)|}dk'\end{aligned}$$

For $k>q$:

$$\begin{aligned}\mathrm{Im}\Pi_{\frac{1}{2},-\frac{3}{2}} = \frac{1}{6561}\Bigg[&\frac{3}{10}q\Big(4617q^5 - 13122q^4\omega_p - 1755q^3\omega_p^2 + 2280q^2\omega_p^3 + 360q\omega_p^4 - 140\omega_p^5\Big) \\ &+ (3q-\omega_p)^3(3q+\omega_p)^2(3q+7\omega_p)\log\left(1 - \frac{6q}{3q+\omega_p}\right)\Bigg] \\ &- \frac{1}{3149280q}\Bigg[(q-\omega_p)\Big(98873q^6 + 194375q^5\omega_p - 147310q^4\omega_p^2 \\ &- 4410q^3\omega_p^3 + 11685q^2\omega_p^4 + 867q\omega_p^5 - 480\omega_p^6\Big) \\ &- 480q(3q-\omega_p)^3(3q+\omega_p)^2(3q+7\omega_p)\log\left(\frac{4q}{3q+\omega_p}\right)\Bigg]\end{aligned}$$

For $k < q$:

$$\begin{aligned}\mathrm{Im}\Pi_{\frac{1}{2},-\frac{3}{2}} = \frac{1}{3149280q}\Bigg[&(q-\omega_p)\Big(98873q^6 + 194375q^5\omega_p - 147310q^4\omega_p^2 \\ &- 4410q^3\omega_p^3 + 11685q^2\omega_p^4 + 867q\omega_p^5 - 480\omega_p^6\Big) \\ &- 480q(3q-\omega_p)^3(3q+\omega_p)^2(3q+7\omega_p)\log\left(\frac{4q}{3q+\omega_p}\right)\Bigg]\end{aligned}$$

Chapter 4

Summary and conclusion

In this research project, we studied the linear response in Rarita-Schwinger-Weyl (RSW) semimetals. Our main objective was to calculate the charge response for RSW semimetals. For this, we used Kubo formula. We analyzed the electronic properties of RSW semimetals of spin-3/2 particles. Subsequently, we attempted to study the system's response to an external electric field under linear response theory. Although our research has not yet fully yielded the charge response due to lack of programming knoowledge, but we have made significant progress in this direction. We have calculate the eigen vector of Hamiltonian $H(\mathbf{k}) = v_0 \left(k_x J_x + k_y J_y + \chi k_z J_z\right)$ and unitary rotational matrix $\langle J_0(\theta_{\mathbf{k},\mathbf{k}+\mathbf{q}})\rangle^2$ for spin-$\frac{3}{2}$ quasiparticle, which provide the basis for calculating the charge response in future work.

With this study we have reached the following conclusions:

- RSW semimetals display unique electronic properties due to spin-3/2 quachaparticles, which makes them different from traditional Weyl and

Dirac semimetals.

- We saw that the charge reaction in RSW semimetals can be calculated using the linear reaction principle, but this process is complex and has additional challenges due to high-spin particles.

- Although we have completed early calculations, the complete etymology of the charge response requires more detailed analysis. In the future, we can study the effects of electron-electron interaction and external regions in non-traditional semimetals.

Bibliography

[1] Renato MA Dantas, Francisco Peña-Benitez, Bitan Roy, and Piotr Surówka. Non-abelian anomalies in multi-weyl semimetals. *Physical Review Research*, 2(1):013007, 2020.

[2] Rahul Ghosh, Firdous Haidar, and Ipsita Mandal. Linear response in planar hall and thermal hall setups for rarita-schwinger-weyl semimetals. *Physical Review B*, 110(24):245113, 2024.

[3] Hongshuang Liu, Jiashuo Liang, Taiyu Sun, and Liying Wang. Recent progress in topological semimetal and its realization in heusler compounds. *Materials Today Physics*, 41:101343, 2024.

[4] Ipsita Mandal. Andreev bound states in superconductor-barrier-superconductor junctions of rarita-schwinger-weyl semimetals. *Physics Letters A*, 503:129410, 2024.

[5] Ganesh Sundaram and Qian Niu. Wave-packet dynamics in slowly perturbed crystals: Gradient corrections and berry-phase effects. *Physical Review B*, 59(23):14915, 1999.

[6] Hongming Weng, Chen Fang, Zhong Fang, B Andrei Bernevig, and Xi Dai. Weyl semimetal phase in noncentrosymmetric transition-metal monophosphides. *Physical Review X*, 5(1):011029, 2015.

[7] Hermann Weyl. Gravitation and the electron. *Proceedings of the National Academy of Sciences*, 15(4):323–334, 1929.

[8] Su-Yang Xu, Ilya Belopolski, Nasser Alidoust, Madhab Neupane, Guang Bian, Chenglong Zhang, Raman Sankar, Guoqing Chang, Zhujun Yuan, Chi-Cheng Lee, et al. Discovery of a weyl fermion semimetal and topological fermi arcs. *Science*, 349(6248):613–617, 2015.

[9] Steve M Young, Saad Zaheer, Jeffrey CY Teo, Charles L Kane, Eugene J Mele, and Andrew M Rappe. Dirac semimetal in three dimensions. *Physical review letters*, 108(14):140405, 2012.